Article

Suppression of NASH-related HCC by farnesyltransferase inhibitor through inhibition of inflammation and hypoxia-inducible factor-1α expression

Kohei Yamada [1], Tomokazu Tanaka [1, *], Keita Kai [2], Shohei Matsufuji [1], Kotaro Ito [1], Yoshihiko Kitajima [1, 3], Tatsuya Manabe [1], and Hirokazu Noshiro [1]

[1] Department of Surgery, Saga University Faculty of Medicine, 5-1-1 Nabeshima, Saga, 849-8501, Japan; 19624021@edu.cc.saga-u.ac.jp (K.Y.); f8642@cc.saga-u.ac.jp (T.T.); 19624016@edu.cc.saga-u.ac.jp (S.M.); sh2806@cc.saga-u.ac.jp (K.I.); kitajima.yoshihiko.eg@mail.hosp.go.jp (Y.K.); manabe@cc.saga-u.ac.jp (T.M.); noshiro@cc.saga-u.ac.jp (H.N.)

[2] Department of Pathology, Saga University Faculty of Medicine, 5-1-1 Nabeshima, Saga, 849-8501, Japan; kaikeit@cc.saga-u.ac.jp (K.K.)

[3] Department of Surgery, National Hospital Organization Higashisaga Hospital, 7324 Harakoga, Miyaki-cho, Miyaki-gun, Saga, 849-0101, Japan

* Correspondence: f8642@cc.saga-u.ac.jp; Tel.: +81-952-34-2349

Abstract: Inflammatory processes play major roles in carcinogenesis and progression of hepatocellular carcinoma (HCC) derived from non-alcoholic steatohepatitis (NASH). But there are no therapies for NASH related HCC, especially focusing on these critical steps. Previous studies reported that farnesyltransferase inhibitors (FTIs) have anti-inflammatory and anti-tumor effects. However, the influence of FTIs on NASH-related HCC has not been elucidated. In HCC cell lines, HepG2, Hep3B, and Huh-7, we confirmed expression of hypoxia-inducible factor (HIF)-1α, an accelerator of tumor aggressiveness and the inflammatory response. We established NASH-related HCC models under inflammation and free fatty acid burden and confirmed that HIF-1α expression was increased under both conditions. Tipifarnib, which is an FTI, strongly suppressed increased HIF-1α, inhibited cell proliferation, and induced apoptosis. Simultaneously, intracellular interleukin-6 as an inflammation marker was increased under both conditions and significantly suppressed by tipifarnib. Additionally, tipifarnib suppressed expression of phosphorylated nuclear factor-κB and transforming growth factor-β. Finally, in a NASH-related HCC mouse model burdened with diethylnitrosamine and a high fat diet, tipifarnib significantly reduced tumor nodule formation in association with decreased serum interleukin-6. In conclusion, tipifarnib has anti-tumor and anti-inflammatory effects in a NASH-related HCC model and may be a promising new agent to treat this disease.

Keywords: non-alcoholic steatohepatitis, hepatocellular carcinoma, farnesyltransferase inhibitor, hypoxia-inducible factor-1α, anti-inflammatory response, nuclear factor-κB, transforming growth factor-β, Warburg effect, reactive oxygen species, interleukin-6

1. Introduction

Obesity has become a prominent health concern worldwide as a risk factor for several chronic diseases, including diabetes mellitus, cardiovascular disease, and chronic kidney disease [1,2]. Besides, obesity is one of the most common and well-documented risk factors for non-alcoholic fatty liver disease (NAFLD) [3]. NAFLD is associated with a relatively low hepatocellular carcinoma (HCC) risk (annual incidence: 0.44 per 1,000 person-years) [4]. However, the incidence of HCC increases up to 5.29 per 1,000 person-years after the transition to non-alcoholic fatty liver disease (NASH) [4]. Vaccination and directly acting anti-viral agents have reduced the risk of virus-induced HCC [5,6]. However,

there are few preventive strategies to stop NASH progression. Weight loss suppresses NASH-related HCC development, but it is difficult to achieve and sustain weight loss [7]. Therefore, another preventative or therapeutic strategy for NASH-related HCC is needed. NASH results from the pathological evolution of NAFLD, following hepatic steatosis. Inflammation in NASH is mainly induced by several cytokines, such as interleukin (IL)-6 and tumor necrosis factor-α (TNF-α), produced by adipocytes and hepatic stellate cells, and gut-derived lipopolysaccharide (LPS) [8–10]. Although previous studies have revealed the effects of free fatty acids and cytokines on hepatocytes during NASH development [11–15], their pathological roles remain unclear in the progression of HCC from NASH.

Farnesyltransferase inhibitors (FTIs) suppress the proliferation of cancer cells such as hematological or head and neck cancers [16–19]. Protein farnesylation is closely associated with inflammatory response and insulin signaling pathways in normal cells [20]. Hepatic steatosis is strongly associated with insulin resistance in the liver and many antidiabetic drugs have been suggested to have a role in treating NAFLD and/or slowing down its progression to NASH and NASH-related HCC as well as improving hyperglycemia in animal studies [21–24]. Thus, we hypothesized that protein farnesylation may be an important therapeutic target in NASH-related HCC, which is based on the chronic inflammation and insulin resistance of hepatocytes.

We and other researchers have shown that hypoxia-inducible factor (HIF)-1α promotes cancer aggressiveness through cancer cell proliferation, invasion, and metastasis [25–28]. HIF-1α is also a major mediator of inflammation that promotes cancer aggressiveness [29,30]. Previously, we demonstrated that 300 nM tipifarnib, which is an FTI, reduces HIF-1α expression in triple-negative breast cancer cells and suppresses migration, cancer stemness, and epithelial-to-mesenchymal transition regardless of RAS expression [31]. Additionally, we have shown that tipifarnib suppresses HIF-1α expression in gastric cancer cells and inhibits their proliferation and migration in vitro and in vivo [27]. Chronic inflammation of hepatocytes results in HCC development from NASH [32,33], but the mechanism remains unknown in relation to HIF-1α and FTIs.

In this study, we initially determined whether tipifarnib affected cell proliferation, metabolic changes, inflammation, and HIF-1α expression in human HCC cell lines cultured under several conditions of cytokines and free fatty acids mimicking the NASH environment. Then, we demonstrated multiple effects of tipifarnib on cancer progression and inflammatory response in a NASH-driven HCC mouse model induced by a high-fat diet and chemical carcinogen.

2. Results

2.1. HIF-1α expression under normoxia

HIF-1α expression was assessed in HepG2, Hep3B, and Huh-7 cells under normoxia. Tipifarnib decreased HIF-1α protein expression in a dose-dependent manner in these cell lines (Figure 1A). HIF-1α expression under 300 nM tipifarnib treatment was significantly decreased, by 51.2% in HepG2 cells, 39.2% in Hep3B cells, and 63.6% in Huh-7 cells (Figure 1B, C). The most suppressive effect of tipifarnib was observed at 300 nM. Therefore, we used 300 nM tipifarnib in the following experiments.

2.2. HIF-1α expression under NASH-like conditions

In HepG2, Hep3B, and Huh-7 cells, treatment with low and moderate concentrations of the cytokine cocktail for 24 h significantly increased HIF-1α expression in a dose-dependent manner. Similarly, HIF-1α expression was increased by palmitic acid (PA) at 50 and 100 μM in HepG2 and Hep3B cells, and 25 and 50 μM in Huh-7 cells in a dose-dependent manner (Figure 2A). Tipifarnib strongly reversed the NASH condition-induced increase of HIF-1α protein expression in these cells (Figure 2B, C and S1).
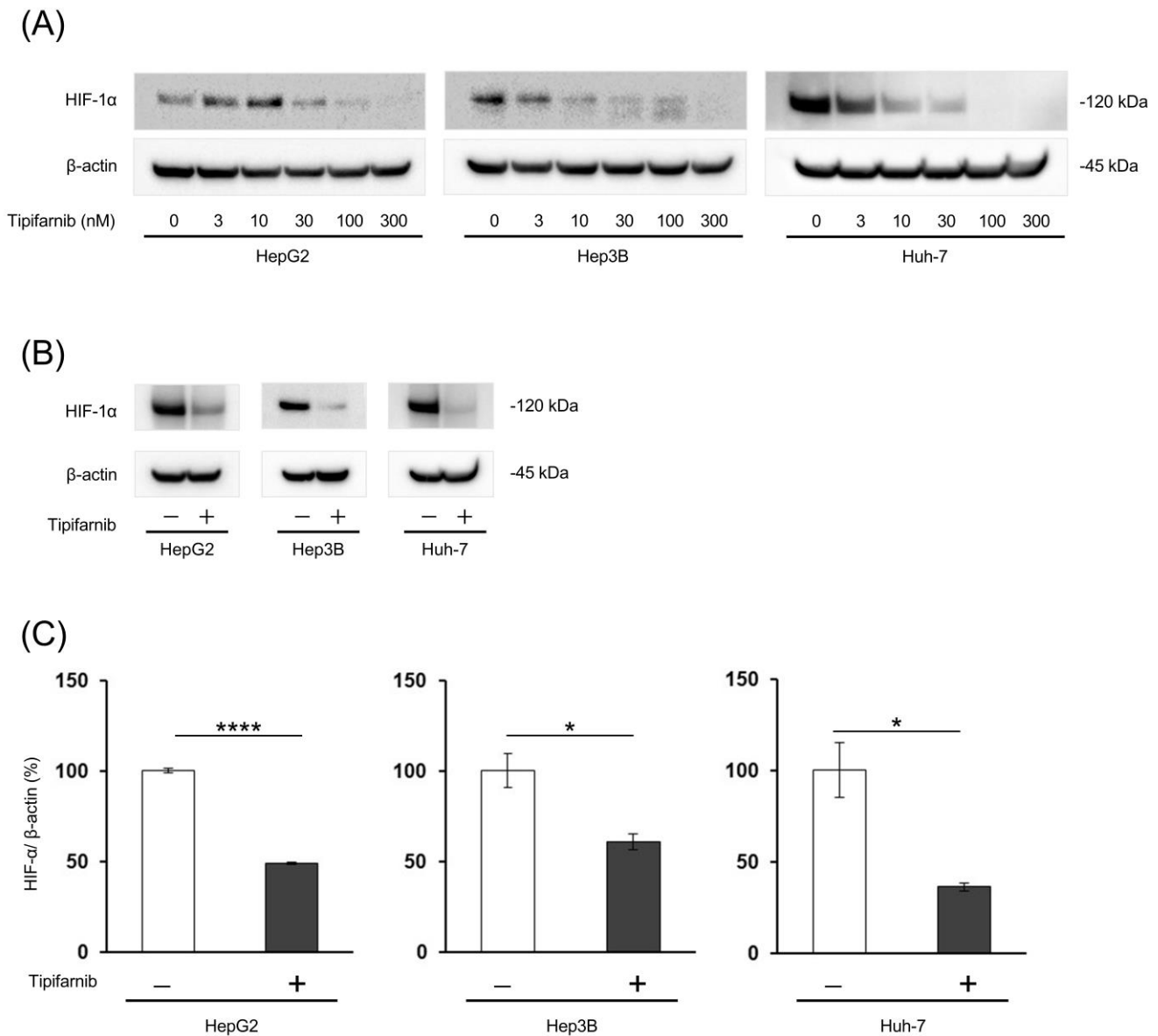
Figure 1. Effect of tipifarnib on hypoxia-inducible factor (HIF)-1α expression in HepG2, Hep3B, and Huh-7 cells. (A) HIF-1α protein expression was decreased in a dose-dependent manner by treatment with tipifarnib for 24 h. (B, C) HIF-1α expression was observed under normoxic conditions in these HCC cell lines. Treatment with 300 nM tipifarnib for 24 h significantly decreased the HIF-1α protein level. β-Actin as an internal reference was equally expressed in these cells. *p < 0.05, ****p < 0.0001 versus control, N.S.: not significant.
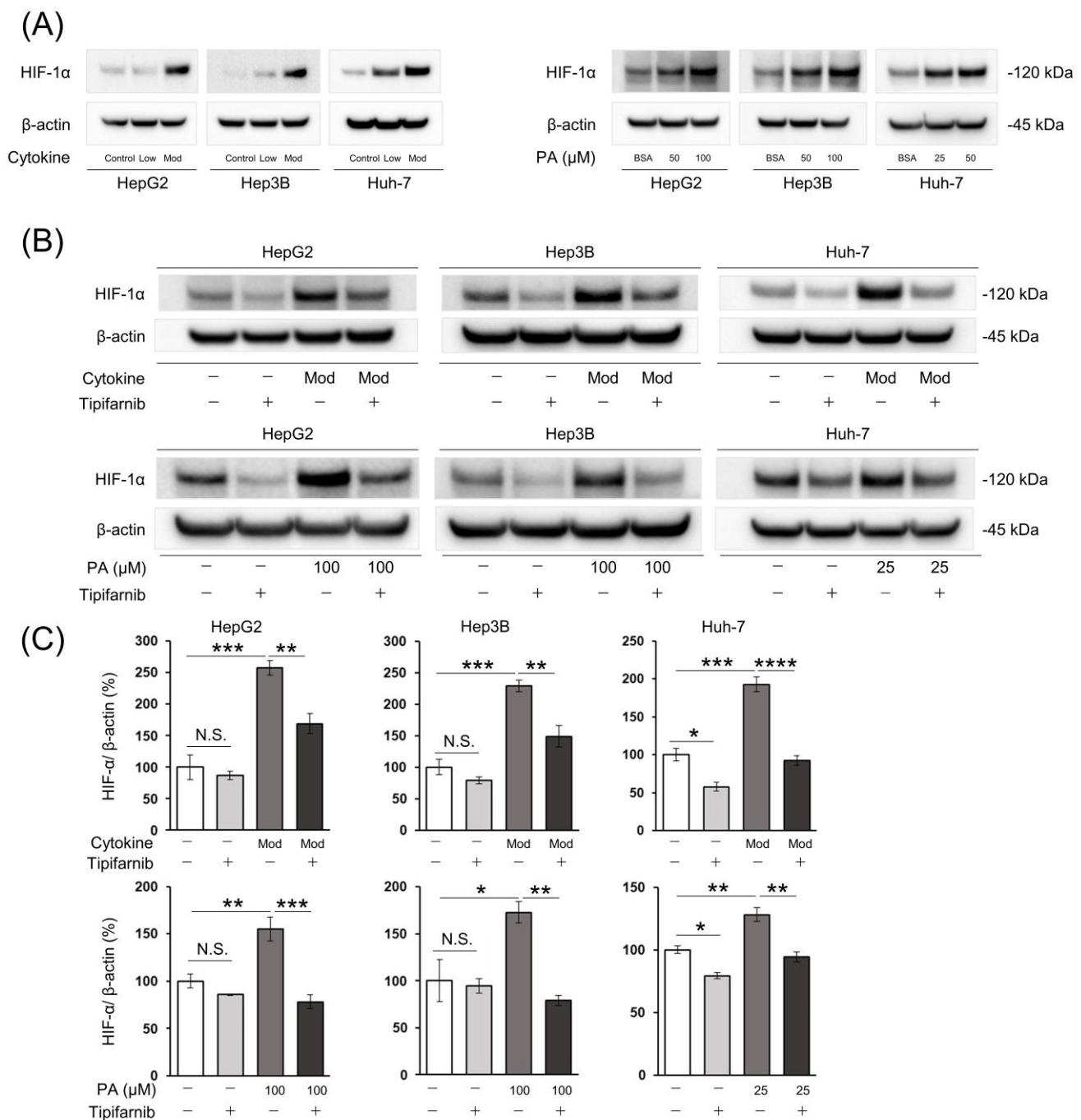
Figure 2. Effect of tipifarnib on HIF-1α expression under inflammation-induced and fatty acid-loaded conditions in HepG2, Hep3B, and Huh-7 cells. (A) HIF-1α expression was increased by treatment with the cytokine cocktail (low and moderate concentrations) and palmitic acid (PA) (HepG2 and Hep3B cells: 50 and 100 μM; Huh-7 cells: 25 and 50 μM) for 24 h in a dose-dependent manner. (B, C) Treatment with tipifarnib (300 nM) for 24 h reversed the increased HIF-1α expression by treatment with the cytokine cocktail (moderate concentration) and PA (HepG2 and Hep3B cells: 100 μM; Huh-7 cells: 25 μM). Mod and Low indicate moderate and low concentrations of the cytokine cocktail, respectively. β-Actin as an internal reference was equally expressed in these cells. Expression under treatment with tipifarnib alone and the cytokine cocktail/PA without tipifarnib was compared with that in the control. Expression under treatment with the cytokine cocktail or PA with tipifarnib was compared with that under treatment with the cytokine cocktail or PA without tipifarnib. *p < 0.05, **p < 0.01, ***p < 0.001, ****p < 0.0001, N.S.: not significant.

2.3. Proliferation of HCC cell lines under NASH-like conditions

In the inflammation-induced model, trypan blue exclusion assays showed that tipifarnib significantly inhibited cell growth under treatment with or without moderate concentrations of the cytokine cocktail at 24-48 h in HepG2 cells and 48 h in Hep3B and Huh-7 cells (Figure 3A). The cell death rate was significantly higher under treatment with the cytokine cocktail and tipifarnib than without tipifarnib at 24–48 h in HepG2 cells and 48 h in Hep3B cells. Additionally, the cell death rate was significantly higher in the cytokine cocktail + tipifarnib group than in the tipifarnib alone group at 48 h in HepG2 and Hep3B cells (Figure S2A). Similarly, in the fatty acid-loaded condition with PA at 100 μM in HepG2 and Hep3B cells and 25 mM in Huh-7 cells, treatment with tipifarnib significantly inhibited cell growth at 24–72 h in HepG2 cells and 72 h in Hep3B and Huh-7 cells (Figure 3B). Cell death rates in the fatty acid-loaded condition with tipifarnib were significantly higher than those without tipifarnib at 24–72 h in Huh-7 cells. Of note, the cytotoxic effect of tipifarnib on cell proliferation was significantly higher in the fatty acid-loaded condition at 24 h in HepG2 cells and 24–72 h in Huh-7 cells (Figure S2B).

2.4. Apoptosis of HCC cell lines under NASH-like conditions

To further investigate the cytotoxic effect of tipifarnib, we examined the expression of cleaved poly(ADP-ribose) polymerase (PARP) in HepG2 and Hep3B cells cultured under the inflammatory condition for 48 h and fatty acid-loaded condition for 72 h in the presence or absence of 300 nM tipifarnib. Western blot analyses revealed cleaved PARP expression in HepG2 and Hep3B cells under the moderate concentrations of the cytokine cocktail + tipifarnib, but not tipifarnib alone for 48 h (Figure 3C). Similarly, cleaved PARP expression was observed under tipifarnib alone and 100 μM PA + tipifarnib for 72 h. However, cleaved PARP expression was significantly higher under treatment with PA + tipifarnib than with tipifarnib alone (Figure 3D). These results indicated that tipifarnib strongly induced apoptosis of HCC cell lines, and the apoptotic effect of tipifarnib was stronger under NASH-like conditions.
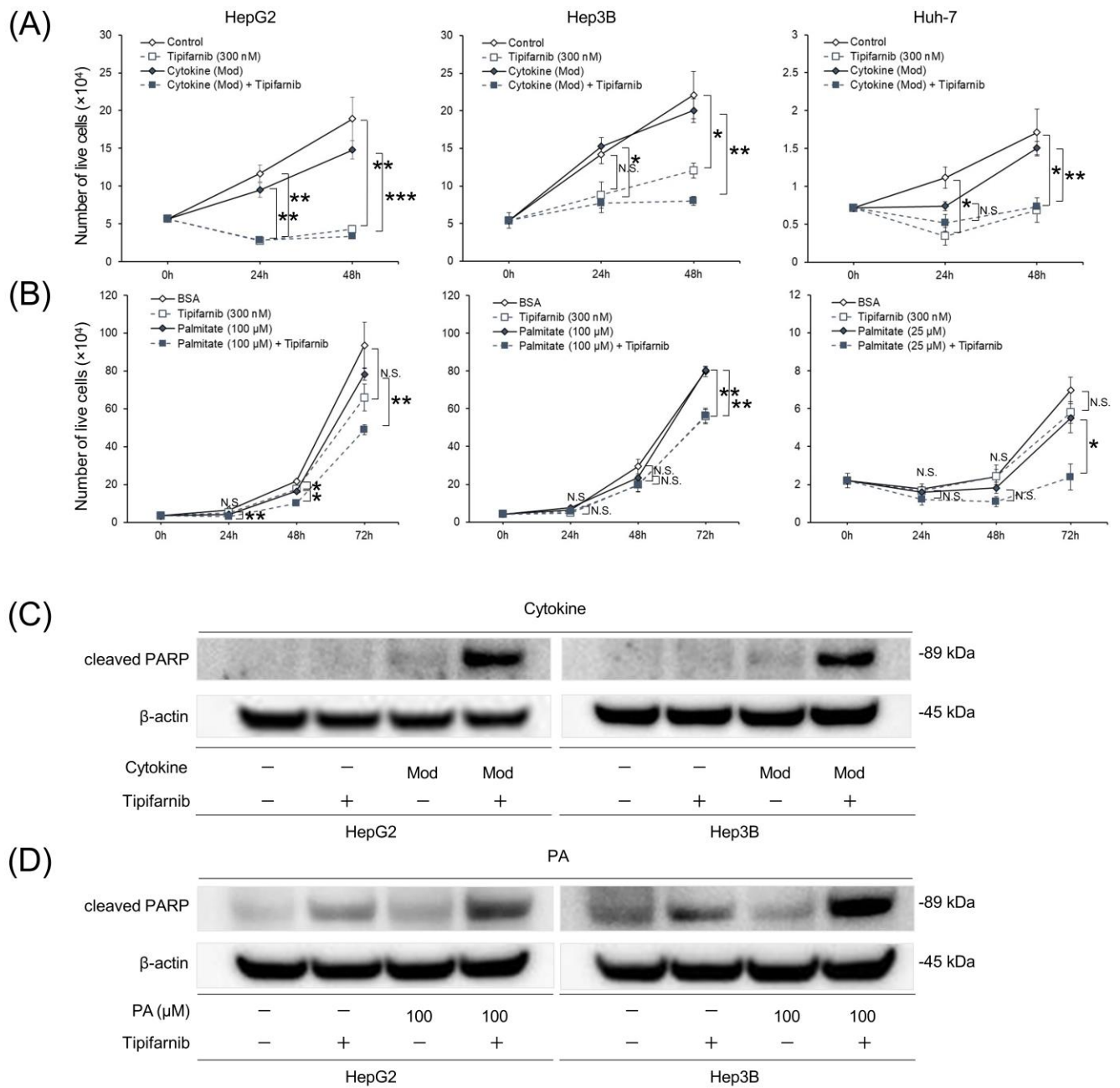
Figure 3. Effect of tipifarnib on cell proliferation and apoptosis under inflammation-induced and fatty acid-loaded conditions in HepG2, Hep3B, and Huh-7 cells. (A) Numbers of live cells were assessed under the inflammation-induced condition (moderate concentrations of the cytokine cocktail) with or without 300 nM tipifarnib for 0–48 h. (B) Numbers of live cells were assessed under the fatty acid-loaded condition (followed by the amount of PA) (HepG2 and Hep3B cells: 100 μM; Huh-7 cells: 25 μM) with or without 300 nM tipifarnib for 0–72 h. (C, D) Western blot analysis of cleaved poly(ADP-ribose) polymerase (PARP) expression was performed in HepG2 and Hep3B cells treated with moderate concentrations of the cytokine cocktail for 48 h (C) and 100 μM PA for 72 h (D) concurrently treated with or without 300 nM tipifarnib. β-Actin as the internal reference was equally expressed in these cells. *$p < 0.05$, **$p < 0.01$, ***$p < 0.001$, control versus tipifarnib alone or cytokine cocktail/PA without tipifarnib versus conditions with tipifarnib, N.S.: not significant.

2.5. Glycolytic metabolism in HCC cells under NASH-like conditions

To investigate whether HIF-1α expression decreased by tipifarnib-attenuated glyco-lytic metabolism, we evaluated the effects of tipifarnib on glucose uptake and lactate

production in HepG2 and Hep3B cells. Glucose uptake was increased in both cell lines treated with the moderate concentrations of the cytokine cocktail as the inflammation-induced condition, particularly by approximately 1.3-fold in Hep3B cells. Tipifarnib significantly decreased glucose uptake even under the inflammation-induced condition and control (Figure 4A). Similarly, tipifarnib decreased lactate production under the inflammation-induced condition, although lactate production in both cell lines was not altered by treatment with the cytokine cocktail (Figure 4B). Glucose uptake by cells treated with 100 µM PA as the fatty acid-loaded condition was also increased, but not significantly. Additionally, glucose uptake was significantly decreased by addition of tipifarnib (Figure 4C). Lactate production was also significantly decreased by tipifarnib, whereas treatment with PA did not affect lactate production in HepG2 and Hep3B cells (Figure 4D). These findings suggested that tipifarnib attenuated glycolytic metabolism in hepatic cancer cell lines cultured under NASH-like conditions and HIF-1α played a major role in regulating this metabolic reprogramming.
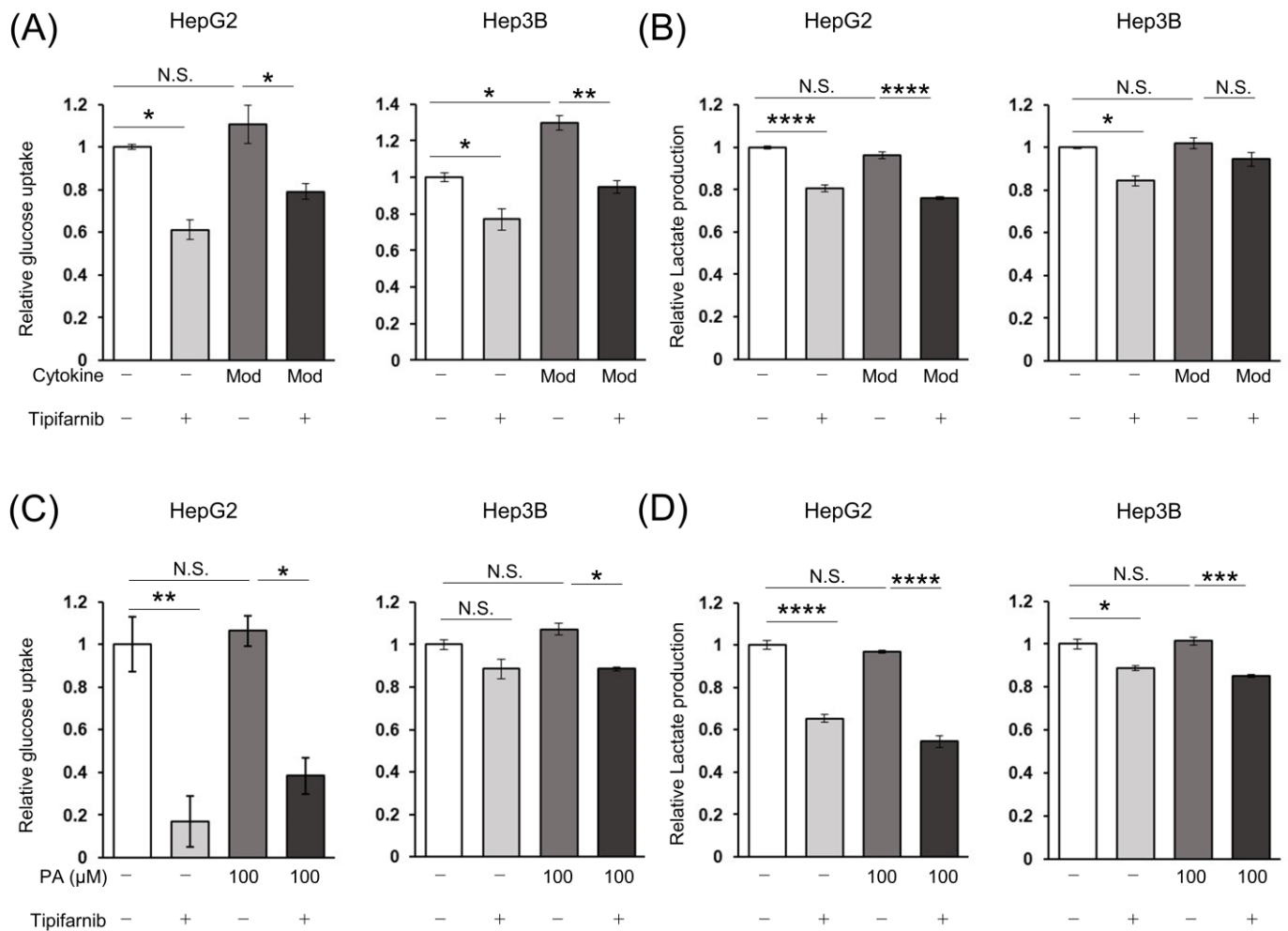
Figure 4. Effects of tipifarnib (300 nM) on glucose uptake and lactate production in HCC cells under non-alcoholic steatohepatitis (NASH)-like conditions. (A, B) Relative glucose uptake (A) and relative lactate production (B) were evaluated in HepG2 and Hep3B cells treated with moderate concentrations of the cytokine cocktail with or without tipifarnib for 48 h. (C, D) Relative glucose uptake (C) and lactate production (D) were evaluated under treatment with 100 μM PA with or without tipifarnib for 48 h. Control levels were set to 1. Levels under treatment with tipifarnib alone (gray bars) and the cytokine cocktail/PA without tipifarnib (dark gray bars) were compared with those in the control (white bars). Levels under treatment with the cytokine cocktail/PA with tipifarnib (black bars) were compared with those under treatment with the cytokine cocktail/PA without tipifarnib. $*p < 0.05$, $**p < 0.01$, $***p < 0.001$, $****p < 0.0001$, N.S.: not significant.

2.6. Reactive oxygen species (ROS) production in HCC cells under NASH-like conditions

We next assessed ROS production underlying the induction of apoptotic cell death by tipifarnib in HepG2, Hep3B, and Huh-7 cells. Tipifarnib significantly increased ROS levels in HepG2 and Hep3B cells treated with or without the moderate concentrations of

the cytokine cocktail. There was a trend of increased ROS levels by tipifarnib in Huh-7 cells regardless of the inflammation-induced condition, although this was not significant (Figure 5A). Similarly, tipifarnib significantly increased the ROS levels in HCC cells treated with or without 100 μM PA in HepG2, Hep3B, and Huh-7 cells. Either the cytokine cocktail or PA did not affect the ROS level in HCC cell lines, whereas the ROS level in HepG2 cells treated with only 100 μM PA was significantly decreased compared with that in the control (Figure 5B).
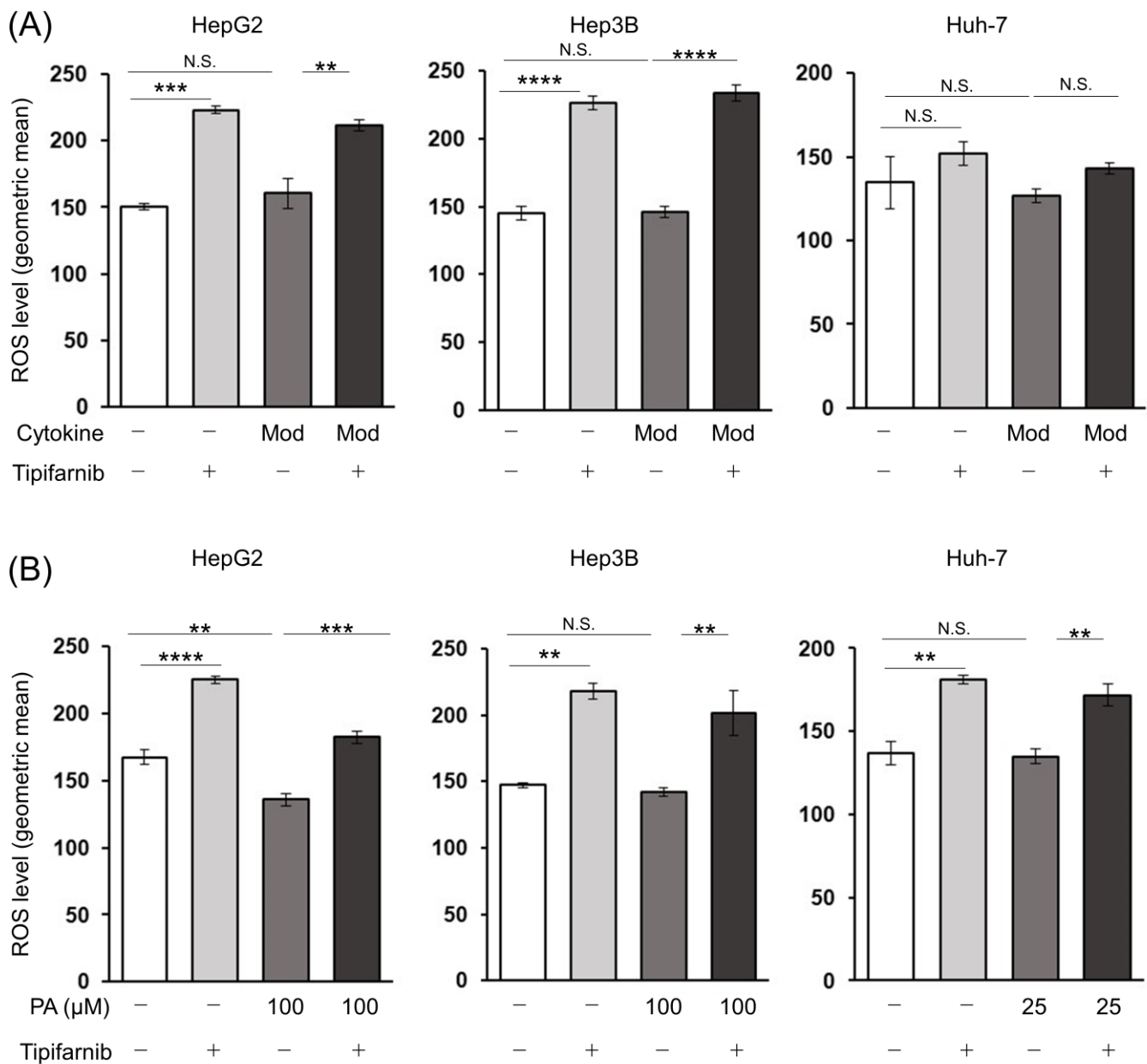

Figure 5. Tipifarnib increases intracellular reactive oxygen species (ROS) production in HepG2, Hep3B, and Huh-7 cells under NASH-like conditions. (A, B) Tipifarnib treatment (300 nM) for 48 h increased the intracellular ROS level in HCC cells treated with moderate concentrations of the cytokine cocktail (A) and 100 μM PA (B). Levels under treatment with tipifarnib alone (gray bars) and the cytokine cocktail/PA without tipifarnib (dark gray bars) were compared with those in the control (white bars). Levels under treatment with the cytokine cocktail/PA with tipifarnib (black bars) were

compared with those under treatment with the cytokine cocktail/PA without tipifarnib. **p < 0.01, ***p < 0.001, ****p < 0.0001, N.S.: not significant.

2.7. Intracellular IL-6 level in HCC cells

To investigate the effects of FTIs other than ameliorating cancer cell proliferation and metabolism, we focused on the inflammatory response in the in vitro NASH-related HCC model. We measured the intracellular IL-6 level by an ELISA to determine whether tipifarnib improved the inflammatory response in HCC cells under NASH-like conditions. Even under the normal condition, tipifarnib significantly decreased the IL-6 level in HepG2 cells compared with that in the control, but not in Hep3B cells. The IL-6 level was significantly increased by the high concentrations of the cytokine cocktail in HepG2 and Hep3B cells. Tipifarnib significantly decreased the elevated level of IL-6 even under the inflammation-induced condition (Figure 6A). Similarly, the IL-6 level was significantly increased by 250 μM PA in HCC cells. Tipifarnib significantly suppressed the increased IL-6 level under the fatty acid-loaded condition, similarly to the inflammation-induced condition (Figure 6B).

2.8. Nuclear factor-κB (NF-κB) and transforming growth factor-β (TGF-β) protein expression in HCC cells

To further investigate the effects of tipifarnib on inflammation in HCC cells under NASH-like conditions, we evaluated the expression of NF-κB and TGF-β, a master mediator of closely linking inflammation and cancer [34,35]. The expression ratio of phosphorylated NF-κB, which was normalized to total NF-κB (p-NF-κB/NF-κB), was significantly increased in HepG2 cells treated with the moderate concentrations of the cytokine cocktail and 100 μM PA, by 208% and 287% compared with control cells, respectively. Tipifarnib markedly inhibited the increase in the p-NF-κB/NF-κB ratio in these cells. There was a trend of the increased p-NF-κB/NF-κB ratio in Hep3B cells under inflammation-induced and fatty acid-loaded conditions, although this was not significant. Tipifarnib decreased the p-NF-κB/NF-κB ratio in Hep3B cells under NASH-like conditions. However, significance was not reached under the inflammation-induced condition (Figure 6C, D, E). Simultaneously, the protein expression level of TGF-β was significantly increased in HepG2 cells under inflammation-induced and fatty acid-loaded conditions. Tipifarnib treatment significantly inhibited the increase in TGF-β protein expression in HepG2 cells despite treatment with the cytokine cocktail or PA. TGF-β expression in Hep3B cells was markedly increased by the moderate concentrations of the cytokine cocktail. Although TGF-β expression in Hep3B cells was increased by 100 μM PA, it was not significant. Tipifarnib markedly decreased the increase in TGF-β expression in Hep3B cells treated with the cytokine cocktail or PA (Figure 6C, D, F).

2.9. NASH-related HCC mouse model

We determined the effects of tipifarnib in the NASH-driven HCC mouse model. Figure 7A shows the experimental design of the diethylnitrosamine (DEN) + choline-deficient, L-amino acid-defined, high fat diet (CDAHFD) mouse model. At week 33, CDAHFD + vehicle mice developed HCC with 100% incidence. No mice were excluded from or died in this study. Representative images of the liver in mice provided standard chow, CDAHFD + vehicle, or CDAHFD + tipifarnib are shown in Figure 7B. Histological examination showed that tumors had the characteristics of HCC: relatively small tumor cells with a high nuclear/cytoplasmic ratio, polymorphism of the nucleus, and coarse chromatin in hematoxylin and eosin staining. These characteristics were ameliorated in the tipifarnib group compared with the DMSO group (Figure 7C). On the liver surface, we macroscopically counted the number of tumors greater than 6 mm in diameter. Tipifarnib treatment significantly reduced the number of tumors (Figure 7D). Similarly, in the microscopic observation of the cut face of the liver, the area ratio of the tumor to the total

liver was reduced by tipifarnib treatment (Figure 7E). To examine the inhibitory effect of tipifarnib on inflammation in vivo, we examined serum IL-6 levels by an ELISA. Compared with the standard chow group, the serum IL-6 level was significantly increased in the CDAHFD + vehicle group. The IL-6 level in the CDAHFD + tipifarnib group was reduced, but without significance (Figure 7F).
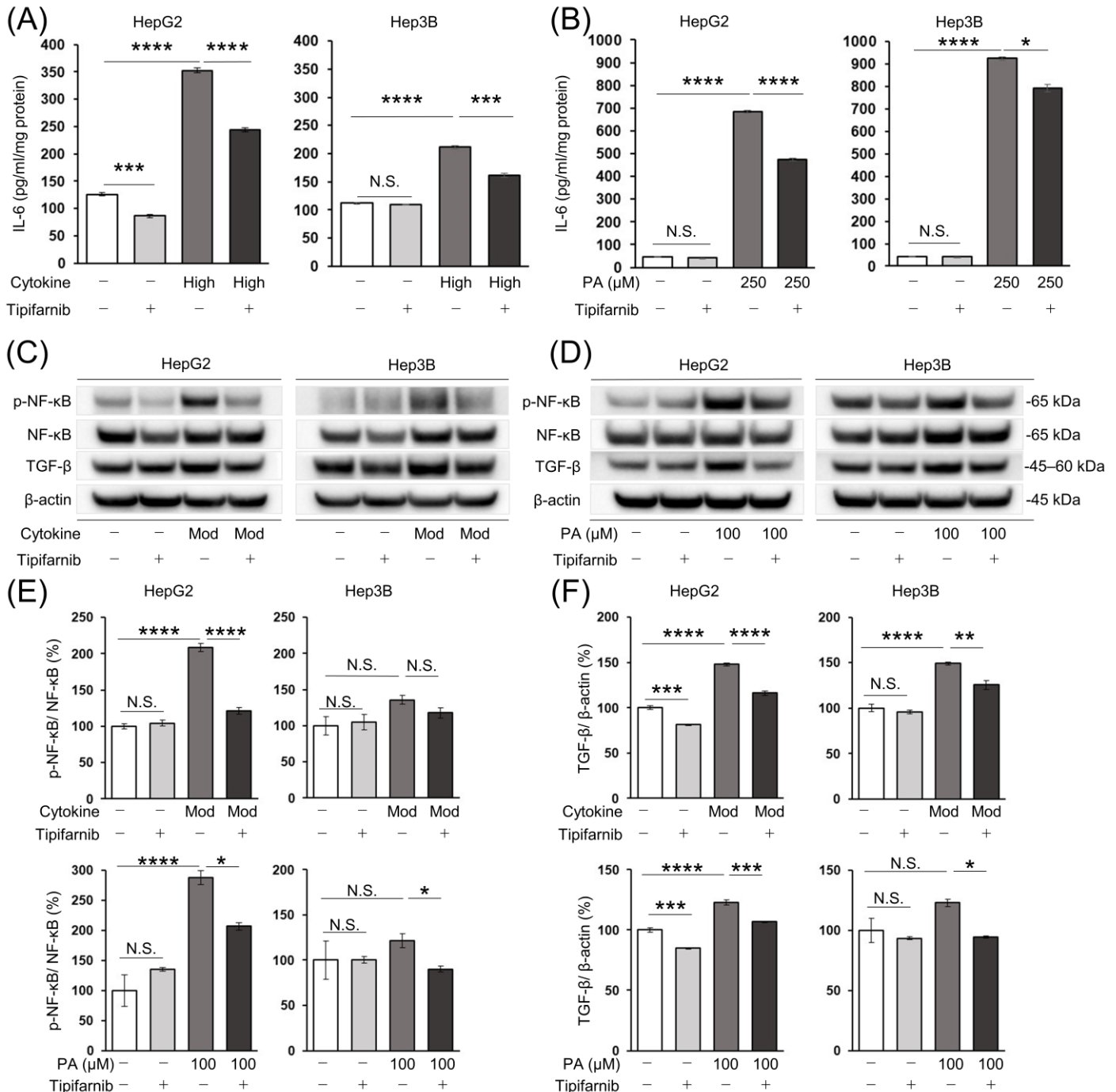

Figure 6. Tipifarnib reverses inflammation in HepG2 and Hep3B cells under NASH-like conditions. (A, B) Tipifarnib treatment (300 nM) for 24 h decreased the increase in intracellular interleukin (IL)-6 in HCC cells treated with high concentrations of the cytokine cocktail (A) and 250 μM PA (B). The IL-6 levels under treatment with tipifarnib alone (gray bars) and the cytokine cocktail/PA without tipifarnib (dark gray bars) were compared with that in the control (white bars). The level under treatment with the cytokine cocktail/PA with tipifarnib (black bars) was compared with that under treatment with the cytokine cocktail/PA without tipifarnib. (C, D) Nuclear factor-κB (NF-κB) and

transforming growth factor-β (TGF-β) expression in HCC cells treated with moderate concentrations of the cytokine cocktail (C) and 100 μM PA (D) with or without tipifarnib (300 nM) for 24 h was detected by western blotting. (E, F) Quantitative analysis of NF-κB (E) and TGF-β (F) protein expression. Levels under treatment with tipifarnib alone (gray bars) and the cytokine cocktail/PA without tipifarnib (dark gray bars) were compared with that in the control (white bars). Levels under treatment with the cytokine cocktail/PA with tipifarnib (black bars) were compared with that under treatment with the cytokine cocktail/PA without tipifarnib. *p < 0.05, **p < 0.01, ***p < 0.001, ****p < 0.0001, N.S.: not significant.
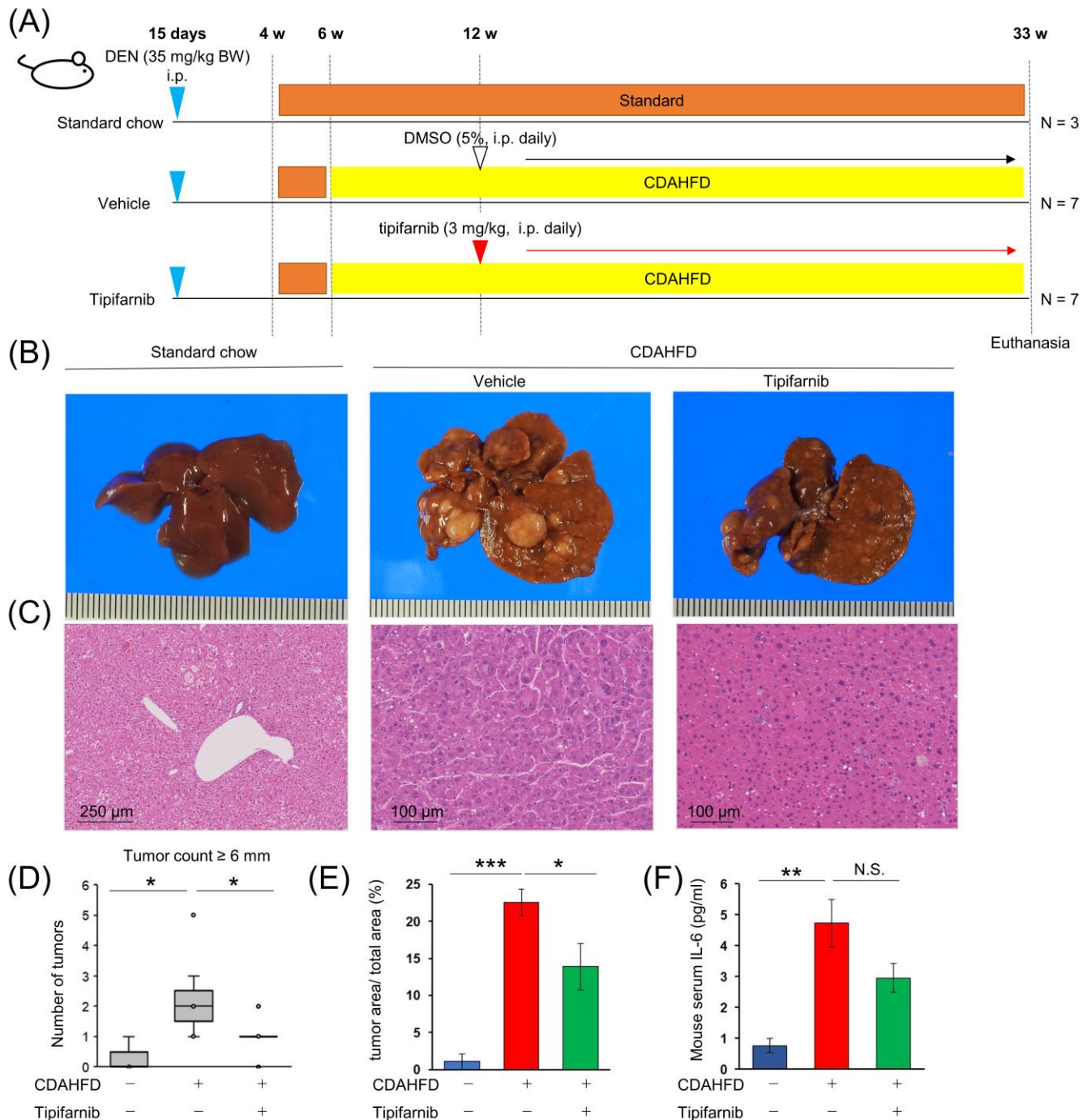

Figure 7. Tipifarnib alleviates HCC progression in the diethylnitrosamine (DEN) + choline-deficient, L-amino acid-defined, high-fat diet (CDAHFD) mouse model. (A) Experimental schema of the DEN + CDAHFD model using male C57/BL/6J mice. DEN (35 mg/kg) was injected intraperitoneally into 15-day-old-mice (blue arrowhead). The mice were weaned at 4 weeks of age, followed by feeding on standard chow (brown bar) or the CDAHFD (yellow bar) after 6 weeks (w) of age for a total of

26 weeks. Either the vehicle (5% DMSO, intraperitoneal, daily; white arrowhead) or tipifarnib (3 mg/kg intraperitoneal, daily; red arrowhead) was administered starting on week 12 and ending on week 33 after birth. All mice were euthanized on week 33 to obtain liver and blood samples. (B) Representative macroscopic images of the liver surface. (C) Representative microscopy images of hematoxylin and eosin (H&E) staining of mouse livers. The image of standard chow-fed mice is normal liver parenchyma. Images of vehicle- and tipifarnib-treated mice show HCC. Scale bars have been added for reference. (D) Numbers of >6 mm macroscopic tumors were counted. (E) Ratio of the cross-sectional area of HCC/total liver was evaluated by a certified pathologist using whole scanned H&E-stained sections of the entire left liver. (F) Mouse serum levels of IL-6 were evaluated by an ELISA. Standard chow group: n = 3 mice; vehicle and tipifarnib group: n = 7 mice. *p < 0.05, **p < 0.01, ***p < 0.001, N.S.: not significant.

3. Discussion

We found that tipifarnib had both anti-tumor and anti-inflammatory effects in HCC cell lines in vitro and in the NASH-related HCC model in vivo. The protein level of HIF-1α was increased in HCC cells cultured under NASH-like conditions, and tipifarnib strongly reversed the expression of HIF-1α. The anti-tumor effects of tipifarnib were closely associated with HIF-1α expression. These findings suggest that HIF-1α plays a major role in cancer aggressiveness of NASH-related HCC.

Hepatic steatosis and inflammation are essential for carcinogenesis in NASH patients and the aggressive phenotype of NASH-related HCC [36–38]. Therefore, we established inflammation-induced and fatty acid-loaded in vitro conditions mimicking NASH. In HCC cell lines under NASH-like conditions, tipifarnib suppressed protein expression of NF-κB and TGF-β, which are associated with inflammation and fibrosis [39–41]. We also found that tipifarnib reduced the IL-6 level elevated by NASH-like conditions in vitro and in vivo. NF-κB regulates IL-6, a major inflammation-associated cytokine that evokes chronic inflammation in the liver [8]. Development of HCC associated with chronic inflammation requires NF-κB signaling in hepatocytes as an anti-apoptotic survival factor [42,43].[44,45] IL-6 mediates signal transducer and activator of transcription 3 (STAT3) activation, which promotes carcinogenesis in the liver. STAT3 is a major driver in the repair and replication of hepatocyte and enhances p300-mediated RelA acetylation, leading to nuclear retention of NF-κB. Thus, persistently activated STAT3 maintains constitutive NF-κB activity in hepatic tumor cells [44]. IL-6 and NF-κB maintain inflammatory responses in the liver, which are followed by development and progression of HCC [34,41,45,46]. We consider that the mechanism of inhibited cancer aggressiveness by tipifarnib under NASH-like conditions may involve inhibition of the vicious cycle of inflammation-promoting cancer and cancer-promoting inflammation.

NASH progression begins by simple steatosis in hepatocytes. Subsequently, interactions between hepatocytes and immune cells such as macrophages and fibroblasts are crucial for the development of hepatitis, fibrosis, and HCC [47–49]. Therefore, development of preventative therapies for NASH-related HCC requires in vitro cellular experiments and in vivo experiments using a NASH-related HCC animal model. Genetic and diet-related animal models are widely used to experimentally simulate the conditions of NASH-related HCC [50–53]. High fat diet-fed mice and genetic mouse models exhibit metabolic syndrome and severe steatosis, but not liver inflammation, fibrosis, or HCC in short-term experiments [54]. A methionine- and choline-deficient (MCD) diet and a CDAHFD both promote liver inflammation and fibrosis. However, the MCD diet model is difficult to apply in long-term experiments leading to carcinogenesis because of severe body weight loss [55]. The mouse model fed the CDAHFD does not related to the problem of weight loss, but this model requires at least 42 weeks to develop regenerative hyperplasia in the liver. Furthermore, the HCC incident rate in microscopic findings is only 27% at 66 weeks [56]. DEN, a highly reactive chemical carcinogen, is widely used to induce HCC in rodents [57]. The combination of CDAHFD feed and DEN injection strongly accelerates carcinogenesis and makes it possible to investigate therapeutic agents for NASH-driven HCC in a state more similar to the mild progression from hepatic steatosis, NAFLD, and NASH

to HCC in a relatively short period [58]. In this study, tipifarnib was administered for 21 weeks, and we observed anti-tumor and anti-inflammatory effects. During the experimental period, significant body weight loss was not observed in the mouse groups treated with or without tipifarnib and no mice died. These results have encouraged us to further investigate clinical application of FTIs in humans with NASH and NASH-related HCC.

To determine whether the anti-tumor effects of tipifarnib were associated with HIF-1α, we focused on energy metabolism, particularly ROS production in cancer cells. ROS has dual contradictory activities in cancer development in accordance with its level: stimulation of tumorigenesis and cancer cell proliferation or induction of cell death [59]. HIF-1α controls ROS production under hypoxic conditions through multiple mechanisms including conversion of energy metabolism from oxidative phosphorylation to glycolysis, which is referred to as the Warburg effect [60–63]. We found that a low dose of tipifarnib suppresses the Warburg effect via HIF-1α in breast and gastric cancer cells under normoxia [27,31]. In the present study, we found that tipifarnib decreased lactate production and glucose consumption, and simultaneously increased ROS production in response to suppressed HIF-1α expression under normoxia. Because tipifarnib induced apoptotic proteins such as cleaved PARP, the excessive ROS production might be involved in the anti-tumor effect of tipifarnib.

Of note, tipifarnib exerted multiple effects in the NASH-related HCC models in vitro and in vivo. An anti-tumor effect was mediated via suppression of HIF-1α, while the others were anti-inflammatory and anti-fibrotic effects such as downregulation of NF-κB, IL-6, and TGF-β. Regarding the anti-tumor effects of tipifarnib, we have reported that tipifarnib also exerts anti-tumor effects through suppression of Rheb farnesylation, leading to inhibition of the mTOR pathway other than via suppression of HIF-1α in gastric cancer cells [27]. In this respect, tipifarnib is speculated to have several mechanisms of anti-tumor effects and is superior to previous HIF-1α inhibitors such as YC-1 and andrographolide [64,65]. Anti-inflammatory effects elicited by tipifarnib have been reported in acute liver failure and burn models in vitro and in vivo [20,66]. These previous reports strongly support our experimental results. Tipifarnib may have the specialized characteristic of simultaneously exerting anti-tumor and anti-inflammatory effects, which is rare for therapeutic agents of cancers. From the viewpoint of these multiple effects of tipifarnib, it may be the most suitable medicine regardless of the timing of administration for NASH-related HCC in which inflammation is deeply involved in its occurrence and development.

In conclusion, tipifarnib is capable of downregulating HIF-1α expression in HCC cells cultured under NASH-like conditions. The tipifarnib-induced decrease in HIF-1α expression is associated with increased ROS production resulting in apoptotic cell death. Tipifarnib-induced decreases in NF-κB and TGF-β expression and the IL-6 level inhibit inflammation–cancer feedback. Thus, tipifarnib is a promising preventative and therapeutic agent for NASH-related HCC.

4. Materials and Methods

4.1. Cell culture

Human HCC cell lines HepG2 and Huh-7 were obtained from the Japanese Cancer Research Resources Bank (Osaka, Japan). Human HCC cell line Hep3B was obtained from the American Type Culture Collection (Manassas, VA, USA). All experiments were performed under normoxia (21% O_2). The cells were cultured and maintained in 4.5 g/l glucose DMEM (Nacalai Tesque, Inc., Kyoto, Japan) supplemented with 10% heat-inactivated fetal bovine serum (FBS; Biowest, Nuaillé, France) and 100 mg/ml kanamycin (Meiji, Tokyo, Japan) at 37°C and 5% CO_2 in a humidified atmosphere.

4.2. Preparation of a palmitic acid (PA)/bovine serum albumin (BSA) complex solution

A palmitic acid stock solution was prepared using a previously described method [67]. Briefly, a 100 mM solution of PA (P0500; Sigma-Aldrich, St. Louis, MO, USA) in 0.1

M NaOH solution (194-02191; FUJIFILM Wako Pure Chemical Corporation) was heated at 70°C in a shaking water bath. In an adjacent water bath, at 55°C, a 10% (w/v) PA-free BSA solution (CultureSure, 034-25462; FUJIFILM Wako Pure Chemical Corporation) was prepared in ddH$_2$O. A 5mM PA/10% (w/v) BSA stock solution was prepared by adding 250 μl of the 100 mM palmitate solution dropwise to 4.75 ml of the 10% (w/v) BSA solution at 55°C, followed by vortex mixing for 10 s and 10 min incubation at 55°C. PA/BSA complex solution was cooled to room temperature and sterile filtered (0.45-μm pore size membrane filter). At the same time, PA-free BSA stock solution was prepared as a control. The complex solution was stored at −20°C, where it is stable for 3–4 weeks. The stored 5mM PA/10% BSA stock solutions were heated for 15min at 55°C and then cooled to room temperature before use.

4.3. Establishment of an in vitro NASH-related HCC model

In vitro culture models of NASH-related HCC were established using a cytokine cocktail and PA. To induce an inflammatory response under hepatitis-like conditions, HepG2, Hep3B, and Huh-7 cells were treated with a cytokine cocktail of TNF-α, interferon-γ (IFN-γ), and LPS (T6674, SRP3058, and L4391, respectively; Sigma-Aldrich). The conditions of the cytokine cocktail were divided into three groups by the final concentrations as follows: (1) high concentrations (0.25 ng/ml TNF-α + 2.5 ng/ml IFN-γ + 0.5 mg/ml LPS); (2) moderate concentrations (0.1 ng/ml TNF-α +1.0 ng/ml IFN-γ + 0.1 mg/ml LPS); (3) low concentrations (0.05 ng/ml TNF-α + 0.5 ng/ml IFN-γ + 0.05 mg/ml LPS). To establish a fat-loaded condition mimicking steatosis, HCC cells were exposed to several concentrations of PA. To determine the effect of tipifarnib (R115777; Selleckchem, Houston, TX, USA) in the in vitro NASH-related HCC models, HCC cells were treated with the cytokine cocktail or PA at several concentrations with or without 300 nM tipifarnib for 24, 48, and 72 h.

4.4. Western blotting

Whole-cell lysates from cultured cells were prepared using lysis buffer composed of 150 nM NaCl, 50 mM Tris-HCl (pH 7.5), 2 mM EDTA, 1% Triton X-100, 1% sodium deoxycholate, 2% sodium dodecyl sulfate, 28 mM phenylmethylsulfonyl fluoride, and a protease inhibitor cocktail mix (Roche, Mannheim, Germany). Aliquots containing 30 mg of protein were electrophoretically separated in 5%–20% Bis-Tris gels (Inter-Techno Co., Ltd.) and transferred to Amersham Hybond P PVDF 0.45 membranes (Cytiva, Tokyo, Japan). Membranes were blocked with 5% skimmed milk at room temperature for 1 h and then incubated overnight at 4°C with the indicated primary antibodies: anti-HIF-1α (1:1,000 dilution, 610958; BD Biosciences), anti-PARP (1:1,000 dilution, 5625S; Cell Signaling Technology, Danvers, MA, USA), anti-NF-κB (1:1,000 dilution, 8242; Cell Signaling Technology), anti-phospho-NF-κB (1:1,000 dilution, 3033S; Cell Signaling Technology), anti-TGF-β (1:1,000 dilution, 3709S; Cell Signaling Technology), and anti-β-actin (1:10,000 dilution, AC15; Sigma-Aldrich). Following incubation with the corresponding secondary antibodies, the signals were developed using ECL Prime Western Blotting Detection Reagent (Cytiva, Tokyo, Japan). Images were acquired using a FUSION FX7.EDGE imaging system (Vilber Bio Imaging, Marne-la-Vallée, France). Densitometry was performed using Evolution-Capt software (Vilber Bio Imaging).

4.5. Cell viability assay

The effect of tipifarnib on cell proliferation was assessed by counting the number of viable cells by a trypan blue exclusion assay using a TC20™ Automated Cell Counter (Bio-Rad, Hercules, CA, USA).

4.6. Measurement of glucose uptake and lactate production

Glucose uptake and lactate production were measured by a Glucose Assay Kit-WST and Lactate Assay Kit-WST (Dojindo Laboratories, Kumamoto, Japan), respectively, in accordance with the manufacturer's instructions.

4.7. Quantification of the intracellular ROS level by flow cytometry

Intracellular ROS levels were measured using a Total ROS Detection Kit (Enzo Life Sciences, Farmingdale, NY, USA), in accordance with the manufacturer's instructions. ROS fluorescence was detected using a FACSVerse flow cytometer (Becton-Dickinson, Franklin Lakes, NJ, USA) and analyzed using FlowJo version 10.0 software (Becton-Dickinson, Franklin Lakes, NJ, USA). The mean fluorescence of ROS production was determined automatically and presented as the geometric mean.

4.8. Measurement of intracellular IL-6 production

Intracellular IL-6 was measured using a Human IL-6 ELISA Kit (RAB0307; Sigma-Aldrich), following the manufacturer's protocol.

4.9. Animal experiments

Animal experimental protocols were approved by the Institutional Animal Care and Use Committee of Saga University (Approval no. A2019-025-0, December 12, 2019). The animals were kept under specific-pathogen-free conditions maintained at 25°C, with relative humidity of 50%, and illuminated by a 12-h light-dark cycle. They were provided with normal or specific sterile food and autoclaved water *ad libitum*. The animal experiments were performed on two or three mice in each cage as the experimental unit. All interventions were carried out during the light cycle. Sample size was determined with power analysis and the HCC incidence rate of mice [58,68]. The mice were excluded from the study when significant body weight loss (≥20%), signs of immobility, ruffled fur, or an inability to eat was observed. The NASH-driven HCC mouse model was established by the method of Li et al [58]. This mouse model develops HCC at 30 weeks of age under a NASH background [58]. Male 7-day-old C57BL/6J mice were obtained from CLEA Japan, Inc. (Tokyo, Japan). A dose of 35 mg/kg diethylnitrosamine (DEN; N0258; Sigma-Aldrich) was injected intraperitoneally into the mice at day 15. At 6 weeks of age, mice were provided either standard chow (n = 3) or a choline-deficient, L-amino acid-defined, high fat diet (CDAHFD) (60 kcal% fat and 0.1% methionine by weight, A06071302; Research Diets, Inc., New Brunswick, NJ, USA) (n = 14) for 26 weeks. After 6 weeks of the CDAHFD, the mice were treated with daily intraperitoneal injections of 3 mg/kg/day tipifarnib (n = 7) or the vehicle [5% DMSO in 0.1 ml normal saline, n = 7] for 21 weeks. The mice were anesthetized for sacrifice. Terminal blood collection was performed by cardiac puncture. The number of liver tumors visible on the surface was counted macroscopically. Then, the left liver lobe was fixed in 3.5% formaldehyde and the right lobe was snap frozen for further analysis.

4.10. Liver histological evaluation

Formaldehyde-fixed samples were examined histologically by hematoxylin and eosin staining. The area of HCC in the total liver of each microscopy image was marked by a certified pathologist blinded to the mouse characteristics. The ratio of the cross-sectional area of HCC to the total liver was calculated using NDP.view2 software (Hamamatsu Photonics, Shizuoka, Japan).

4.11. Measurement of mouse serum IL-6

The mouse serum level of IL-6 was measured using a mouse IL-6 ELISA Kit (RAB0308; Sigma-Aldrich), following the manufacturer's protocol.

4.12. Statistical analysis

Data were analyzed using JMP Pro version 16 (SAS Institute, Inc., Cary, NC, USA). The data were analyzed using the unpaired, two-tailed Student's t-test when comparing two groups. To compare three or more groups, Tukey's multiple comparisons test was performed for one-way ANOVA. $P < 0.05$ was considered statistically significant. All data are expressed as the mean ± SEM.

References

1. Singh, G.M.; Danaei, G.; Farzadfar, F.; Stevens, G.A.; Woodward, M.; Wormser, D.; Kaptoge, S.; Whitlock, G.; Qiao, Q.; Lewington, S.; et al. The age-specific quantitative effects of metabolic risk factors on cardiovascular diseases and diabetes: a pooled analysis. *PLoS ONE* **2013**, *8*, e65174, doi:10.1371/journal.pone.0065174.

2. GBD 2015 Obesity Collaborators; Afshin, A.; Forouzanfar, M.H.; Reitsma, M.B.; Sur, P.; Estep, K.; Lee, A.; Marczak, L.; Mokdad, A.H.; Moradi-Lakeh, M.; Naghavi, M.; et al. Health Effects of Overweight and Obesity in 195 Countries over 25 Years. *N. Engl. J. Med.* **2017**, *377*, 13–27, doi:10.1056/NEJMoa1614362.

3. Subichin, M.; Clanton, J.; Makuszewski, M.; Bohon, A.; Zografakis, J.G.; Dan, A. Liver disease in the morbidly obese: a review of 1000 consecutive patients undergoing weight loss surgery. *Surg. Obes. Relat. Dis.* **2015**, *11*, 137–141, doi:10.1016/j.soard.2014.06.015.

4. Younossi, Z.M.; Koenig, A.B.; Abdelatif, D.; Fazel, Y.; Henry, L.; Wymer, M. Global epidemiology of nonalcoholic fatty liver disease-Meta-analytic assessment of prevalence, incidence, and outcomes. *Hepatology* **2016**, *64*, 73–84, doi:10.1002/hep.28431.

5. Carrat, F.; Fontaine, H.; Dorival, C.; Simony, M.; Diallo, A.; Hezode, C.; De Ledinghen, V.; Larrey, D.; Haour, G.; Bronowicki, J.-P.; et al. Clinical outcomes in patients with chronic hepatitis C after direct-acting antiviral treatment: a prospective cohort study. *Lancet* **2019**, *393*, 1453–1464, doi:10.1016/S0140-6736(18)32111-1.

6. Liao, S.-H.; Chen, C.-L.; Hsu, C.-Y.; Chien, K.-L.; Kao, J.-H.; Chen, P.-J.; Chen, T.H.-H.; Chen, C.-H. Long-term effectiveness of population-wide multifaceted interventions for hepatocellular carcinoma in Taiwan. *J. Hepatol.* **2021**, *75*, 132–141, doi:10.1016/j.jhep.2021.02.029.

7. Rinella, M.E. Nonalcoholic fatty liver disease: a systematic review. *JAMA* **2015**, *313*, 2263–2273, doi:10.1001/jama.2015.5370.

8. Park, E.J.; Lee, J.H.; Yu, G.-Y.; He, G.; Ali, S.R.; Holzer, R.G.; Osterreicher, C.H.; Takahashi, H.; Karin, M. Dietary and genetic obesity promote liver inflammation and tumorigenesis by enhancing IL-6 and TNF expression. *Cell* **2010**, *140*, 197–208, doi:10.1016/j.cell.2009.12.052.

9. Krawczyk, M.; Bonfrate, L.; Portincasa, P. Nonalcoholic fatty liver disease. *Best Pract. Res. Clin. Gastroenterol.* **2010**, *24*, 695–708, doi:10.1016/j.bpg.2010.08.005.

10. Drucker, C.; Parzefall, W.; Teufelhofer, O.; Grusch, M.; Ellinger, A.; Schulte-Hermann, R.; Grasl-Kraupp, B. Non-parenchymal liver cells support the growth advantage in the first stages of hepatocarcinogenesis. *Carcinogenesis* **2006**, *27*, 152–161, doi:10.1093/carcin/bgi202.

11. Takaki, A.; Kawai, D.; Yamamoto, K. Multiple hits, including oxidative stress, as pathogenesis and treatment target in non-alcoholic steatohepatitis (NASH). *Int. J. Mol. Sci.* **2013**, *14*, 20704–20728, doi:10.3390/ijms141020704.

12. Csak, T.; Ganz, M.; Pespisa, J.; Kodys, K.; Dolganiuc, A.; Szabo, G. Fatty acid and endotoxin activate inflammasomes in mouse hepatocytes that release danger signals to stimulate immune cells. *Hepatology* **2011**, *54*, 133–144, doi:10.1002/hep.24341.

13. Shimizu, Y.; Tamura, T.; Kemmochi, A.; Owada, Y.; Ozawa, Y.; Hisakura, K.; Matsuzaka, T.; Shimano, H.; Nakano, N.; Sakashita, S.; et al. Oxidative stress and LXR agonist induce hepatocellular carcinoma in NASH model. *J. Gastroenterol. Hepatol.* **2020**, doi:10.1111/jgh.15239.

14. Vecchione, G.; Grasselli, E.; Cioffi, F.; Baldini, F.; Oliveira, P.J.; Sardão, V.A.; Cortese, K.; Lanni, A.; Voci, A.; Portincasa, P.; Vergani, L. The Nutraceutic Silybin Counteracts Excess Lipid Accumulation and Ongoing Oxidative Stress in an In Vitro Model of Non-Alcoholic Fatty Liver Disease Progression. *Front. Nutr.* **2017**, *4*, 42, doi:10.3389/fnut.2017.00042.

15. Oh, J.M.; Choi, J.M.; Lee, J.Y.; Oh, S.J.; Kim, H.C.; Kim, B.H.; Ma, J.Y.; Kim, S.K. Effects of palmitic acid on TNF-α-induced cytotoxicity in SK-Hep-1 cells. *Toxicol In Vitro* **2012**, *26*, 783–790, doi:10.1016/j.tiv.2012.05.013.

16. Dai, Y.; Chen, S.; Pei, X.-Y.; Almenara, J.A.; Kramer, L.B.; Venditti, C.A.; Dent, P.; Grant, S. Interruption of the Ras/MEK/ERK signaling cascade enhances Chk1 inhibitor-induced DNA damage in vitro and in vivo in human multiple myeloma cells. *Blood* **2008**, *112*, 2439–2449, doi:10.1182/blood-2008-05-159392.

17. Lee, K.H.; Koh, M.; Moon, A. Farnesyl transferase inhibitor FTI-277 inhibits breast cell invasion and migration by blocking H-Ras activation. *Oncol. Lett.* **2016**, *12*, 2222–2226, doi:10.3892/ol.2016.4837.

18. Untch, B.R.; Dos Anjos, V.; Garcia-Rendueles, M.E.R.; Knauf, J.A.; Krishnamoorthy, G.P.; Saqcena, M.; Bhanot, U.K.; Socci, N.D.; Ho, A.L.; Ghossein, R.; Fagin, J.A. Tipifarnib Inhibits HRAS-Driven Dedifferentiated Thyroid Cancers. *Cancer Res.* **2018**, *78*, 4642–4657, doi:10.1158/0008-5472.CAN-17-1925.

19. Gilardi, M.; Wang, Z.; Proietto, M.; Chillà, A.; Calleja-Valera, J.L.; Goto, Y.; Vanoni, M.; Janes, M.R.; Mikulski, Z.; Gualberto, A.; et al. Tipifarnib as a Precision Therapy for HRAS-Mutant Head and Neck Squamous Cell Carcinomas. *Mol. Cancer Ther.* **2020**, *19*, 1784–1796, doi:10.1158/1535-7163.MCT-19-0958.

20. Nakazawa, H.; Yamada, M.; Tanaka, T.; Kramer, J.; Yu, Y.-M.; Fischman, A.J.; Martyn, J.A.J.; Tompkins, R.G.; Kaneki, M. Role of protein farnesylation in burn-induced metabolic derangements and insulin resistance in mouse skeletal muscle. *PLoS ONE* **2015**, *10*, e0116633, doi:10.1371/journal.pone.0116633.

21. Seppälä-Lindroos, A.; Vehkavaara, S.; Häkkinen, A.-M.; Goto, T.; Westerbacka, J.; Sovijärvi, A.; Halavaara, J.; Yki-Järvinen, H. Fat accumulation in the liver is associated with defects in insulin suppression of glucose production and serum free fatty acids independent of obesity in normal men. *J. Clin. Endocrinol. Metab.* **2002**, *87*, 3023–3028, doi:10.1210/jcem.87.7.8638.

22. Yoshioka, N.; Tanaka, M.; Ochi, K.; Watanabe, A.; Ono, K.; Sawada, M.; Ogi, T.; Itoh, M.; Ito, A.; Shiraki, Y.; et al. The sodium-glucose cotransporter-2 inhibitor Tofogliflozin prevents the progression of nonalcoholic steatohepatitis-associated liver tumors in a novel murine model. *Biomed. Pharmacother.* **2021**, *140*, 111738, doi:10.1016/j.biopha.2021.111738.

23. Jojima, T.; Wakamatsu, S.; Kase, M.; Iijima, T.; Maejima, Y.; Shimomura, K.; Kogai, T.; Tomaru, T.; Usui, I.; Aso, Y. The SGLT2 Inhibitor Canagliflozin Prevents Carcinogenesis in a Mouse Model of Diabetes and Non-Alcoholic Steatohepatitis-Related Hepatocarcinogenesis: Association with SGLT2 Expression in Hepatocellular Carcinoma. *Int. J. Mol. Sci.* **2019**, *20*, doi:10.3390/ijms20205237.

24. Fruci, B.; Giuliano, S.; Mazza, A.; Malaguarnera, R.; Belfiore, A. Nonalcoholic Fatty liver: a possible new target for type 2 diabetes prevention and treatment. *Int. J. Mol. Sci.* **2013**, *14*, 22933–22966, doi:10.3390/ijms141122933.

25. Kamat, C.D.; Green, D.E.; Warnke, L.; Thorpe, J.E.; Ceriello, A.; Ihnat, M.A. Mutant p53 facilitates pro-angiogenic, hyperpro-liferative phenotype in response to chronic relative hypoxia. *Cancer Lett.* **2007**, *249*, 209–219, doi:10.1016/j.canlet.2006.08.017.

26. Wong, C.C.-L.; Gilkes, D.M.; Zhang, H.; Chen, J.; Wei, H.; Chaturvedi, P.; Fraley, S.I.; Wong, C.-M.; Khoo, U.-S.; Ng, I.O.-L.; Wirtz, D.; Semenza, G.L. Hypoxia-inducible factor 1 is a master regulator of breast cancer metastatic niche formation. *Proc Natl Acad Sci USA* **2011**, *108*, 16369–16374, doi:10.1073/pnas.1113483108.

27. Egawa, N.; Tanaka, T.; Matsufuji, S.; Yamada, K.; Ito, K.; Kitagawa, H.; Okuyama, K.; Kitajima, Y.; Noshiro, H. Antitumor effects of low-dose tipifarnib on the mTOR signaling pathway and reactive oxygen species production in HIF-1α-expressing gastric cancer cells. *FEBS Open Bio* **2021**, *11*, 1465–1475, doi:10.1002/2211-5463.13154.

28. Ito, K.; Kitajima, Y.; Kai, K.; Matsufuji, S.; Yamada, K.; Egawa, N.; Kitagawa, H.; Okuyama, K.; Tanaka, T.; Noshiro, H. Matrix metalloproteinase-1 expression is regulated by HIF-1-dependent and epigenetic mechanisms and serves a tumor-suppressive role in gastric cancer progression. *Int. J. Oncol.* **2021**, *59*, doi:10.3892/ijo.2021.5282.

29. Bruning, U.; Fitzpatrick, S.F.; Frank, T.; Birtwistle, M.; Taylor, C.T.; Cheong, A. NFκB and HIF display synergistic behaviour during hypoxic inflammation. *Cell. Mol. Life Sci.* **2012**, *69*, 1319–1329, doi:10.1007/s00018-011-0876-2.

30. Maxwell, P.J.; Gallagher, R.; Seaton, A.; Wilson, C.; Scullin, P.; Pettigrew, J.; Stratford, I.J.; Williams, K.J.; Johnston, P.G.; Waugh, D.J.J. HIF-1 and NF-kappaB-mediated upregulation of CXCR1 and CXCR2 expression promotes cell survival in hypoxic prostate cancer cells. *Oncogene* **2007**, *26*, 7333–7345, doi:10.1038/sj.onc.1210536.

31. Tanaka, T.; Ikegami, Y.; Nakazawa, H.; Kuriyama, N.; Oki, M.; Hanai, J.-I.; Sukhatme, V.P.; Kaneki, M. Low-Dose Farnesyl-transferase Inhibitor Suppresses HIF-1α and Snail Expression in Triple-Negative Breast Cancer MDA-MB-231 Cells In Vitro. *J. Cell. Physiol.* **2017**, *232*, 192–201, doi:10.1002/jcp.25411.

32. Green, C.D.; Weigel, C.; Brown, R.D.R.; Bedossa, P.; Dozmorov, M.; Sanyal, A.J.; Spiegel, S. A new preclinical model of western diet-induced progression of non-alcoholic steatohepatitis to hepatocellular carcinoma. *FASEB J.* **2022**, *36*, e22372, doi:10.1096/fj.202200346R.

33. Shriki, A.; Lanton, T.; Sonnenblick, A.; Levkovitch-Siany, O.; Eidelshtein, D.; Abramovitch, R.; Rosenberg, N.; Pappo, O.; El-gavish, S.; Nevo, Y.; et al. Multiple roles of IL6 in hepatic injury, steatosis, and senescence aggregate to suppress tumorigenesis. *Cancer Res.* **2021**, *81*, 4766–4777, doi:10.1158/0008-5472.CAN-21-0321.

34. Luedde, T.; Schwabe, R.F. NF-κB in the liver--linking injury, fibrosis and hepatocellular carcinoma. *Nat. Rev. Gastroenterol. Hepatol.* **2011**, *8*, 108–118, doi:10.1038/nrgastro.2010.213.

35. Chen, J.; Gingold, J.A.; Su, X. Immunomodulatory TGF-β Signaling in Hepatocellular Carcinoma. *Trends Mol. Med.* **2019**, *25*, 1010–1023, doi:10.1016/j.molmed.2019.06.007.

36. Yang, Y.M.; Kim, S.Y.; Seki, E. Inflammation and liver cancer: molecular mechanisms and therapeutic targets. *Semin. Liver Dis.* **2019**, *39*, 26–42, doi:10.1055/s-0038-1676806.

37.   Chavez-Tapia, N.C.; Rosso, N.; Tiribelli, C. Effect of intracellular lipid accumulation in a new model of non-alcoholic fatty liver disease. *BMC Gastroenterol.* **2012**, *12*, 20, doi:10.1186/1471-230X-12-20.

38.   Shen, C.; Chen, J.H.; Oh, H.R.; Park, J.H. Transcription factor SOX2 contributes to nonalcoholic fatty liver disease development by regulating the expression of the fatty acid transporter CD36. *FEBS Lett.* **2021**, *595*, 2493–2503, doi:10.1002/1873-3468.14193.

39.   Walton, K.L.; Johnson, K.E.; Harrison, C.A. Targeting TGF-β Mediated SMAD Signaling for the Prevention of Fibrosis. *Front. Pharmacol.* **2017**, *8*, 461, doi:10.3389/fphar.2017.00461.

40.   Xu, L.; Zhang, Y.; Ji, N.; Du, Y.; Jia, T.; Wei, S.; Wang, W.; Zhang, S.; Chen, W. Tanshinone IIA regulates the TGF-β1/Smad signaling pathway to ameliorate non-alcoholic steatohepatitis-related fibrosis. *Exp. Ther. Med.* **2022**, *24*, 486, doi:10.3892/etm.2022.11413.

41.   Xu, X.; Lei, Y.; Chen, L.; Zhou, H.; Liu, H.; Jiang, J.; Yang, Y.; Wu, B. Phosphorylation of NF-κBp65 drives inflammation-mediated hepatocellular carcinogenesis and is a novel therapeutic target. *J. Exp. Clin. Cancer Res.* **2021**, *40*, 253, doi:10.1186/s13046-021-02062-x.

42.   Haybaeck, J.; Zeller, N.; Wolf, M.J.; Weber, A.; Wagner, U.; Kurrer, M.O.; Bremer, J.; Iezzi, G.; Graf, R.; Clavien, P.-A.; et al. A lymphotoxin-driven pathway to hepatocellular carcinoma. *Cancer Cell* **2009**, *16*, 295–308, doi:10.1016/j.ccr.2009.08.021.

43.   Pikarsky, E.; Porat, R.M.; Stein, I.; Abramovitch, R.; Amit, S.; Kasem, S.; Gutkovich-Pyest, E.; Urieli-Shoval, S.; Galun, E.; Ben-Neriah, Y. NF-kappaB functions as a tumour promoter in inflammation-associated cancer. *Nature* **2004**, *431*, 461–466, doi:10.1038/nature02924.

44.   He, G.; Karin, M. NF-κB and STAT3 - key players in liver inflammation and cancer. *Cell Res.* **2011**, *21*, 159–168, doi:10.1038/cr.2010.183.

45.   Makino, Y.; Hikita, H.; Kato, S.; Sugiyama, M.; Shigekawa, M.; Sakamoto, T.; Sasaki, Y.; Murai, K.; Sakane, S.; Kodama, T.; et al. STAT3 is Activated by CTGF-mediated Tumor-stroma Cross Talk to Promote HCC Progression. *Cell. Mol. Gastroenterol. Hepatol.* **2023**, *15*, 99–119, doi:10.1016/j.jcmgh.2022.09.006.

46.   Hoesel, B.; Schmid, J.A. The complexity of NF-κB signaling in inflammation and cancer. *Mol. Cancer* **2013**, *12*, 86, doi:10.1186/1476-4598-12-86.

47.   Novo, E.; Cappon, A.; Villano, G.; Quarta, S.; Cannito, S.; Bocca, C.; Turato, C.; Guido, M.; Maggiora, M.; Protopapa, F.; et al. SerpinB3 as a Pro-Inflammatory Mediator in the Progression of Experimental Non-Alcoholic Fatty Liver Disease. *Front. Immunol.* **2022**, *13*, 910526, doi:10.3389/fimmu.2022.910526.

48.   Yamagishi, R.; Kamachi, F.; Nakamura, M.; Yamazaki, S.; Kamiya, T.; Takasugi, M.; Cheng, Y.; Nonaka, Y.; Yukawa-Muto, Y.; Thuy, L.T.T.; et al. Gasdermin D-mediated release of IL-33 from senescent hepatic stellate cells promotes obesity-associated hepatocellular carcinoma. *Sci. Immunol.* **2022**, *7*, eabl7209, doi:10.1126/sciimmunol.abl7209.

49.   Ploeger, C.; Schreck, J.; Huth, T.; Fraas, A.; Albrecht, T.; Charbel, A.; Ji, J.; Singer, S.; Breuhahn, K.; Pusch, S.; et al. STAT1 and STAT3 Exhibit a Crosstalk and Are Associated with Increased Inflammation in Hepatocellular Carcinoma. *Cancers (Basel)* **2022**, *14*, doi:10.3390/cancers14051154.

50.   Fujii, M.; Shibazaki, Y.; Wakamatsu, K.; Honda, Y.; Kawauchi, Y.; Suzuki, K.; Arumugam, S.; Watanabe, K.; Ichida, T.; Asakura, H.; Yoneyama, H. A murine model for non-alcoholic steatohepatitis showing evidence of association between diabetes and hepatocellular carcinoma. *Med. Mol. Morphol.* **2013**, *46*, 141–152, doi:10.1007/s00795-013-0016-1.

51.   Asgharpour, A.; Cazanave, S.C.; Pacana, T.; Seneshaw, M.; Vincent, R.; Banini, B.A.; Kumar, D.P.; Daita, K.; Min, H.-K.; Mirshahi, F.; et al. A diet-induced animal model of non-alcoholic fatty liver disease and hepatocellular cancer. *J. Hepatol.* **2016**, *65*, 579–588, doi:10.1016/j.jhep.2016.05.005.

52.   Saxena, N.K.; Ikeda, K.; Rockey, D.C.; Friedman, S.L.; Anania, F.A. Leptin in hepatic fibrosis: evidence for increased collagen production in stellate cells and lean littermates of ob/ob mice. *Hepatology* **2002**, *35*, 762–771, doi:10.1053/jhep.2002.32029.

53.   Sahai, A.; Malladi, P.; Pan, X.; Paul, R.; Melin-Aldana, H.; Green, R.M.; Whitington, P.F. Obese and diabetic db/db mice develop marked liver fibrosis in a model of nonalcoholic steatohepatitis: role of short-form leptin receptors and osteopontin. *Am. J. Physiol. Gastrointest. Liver Physiol.* **2004**, *287*, G1035-43, doi:10.1152/ajpgi.00199.2004.

54.   Nevzorova, Y.A.; Boyer-Diaz, Z.; Cubero, F.J.; Gracia-Sancho, J. Animal models for liver disease - A practical approach for translational research. *J. Hepatol.* **2020**, *73*, 423–440, doi:10.1016/j.jhep.2020.04.011.

55.   Farrell, G.; Schattenberg, J.M.; Leclercq, I.; Yeh, M.M.; Goldin, R.; Teoh, N.; Schuppan, D. Mouse models of nonalcoholic steatohepatitis: toward optimization of their relevance to human nonalcoholic steatohepatitis. *Hepatology* **2019**, *69*, 2241–2257, doi:10.1002/hep.30333.

56.   Ikawa-Yoshida, A.; Matsuo, S.; Kato, A.; Ohmori, Y.; Higashida, A.; Kaneko, E.; Matsumoto, M. Hepatocellular carcinoma in a mouse model fed a choline-deficient, L-amino acid-defined, high-fat diet. *Int. J. Exp. Pathol.* **2017**, *98*, 221–233, doi:10.1111/iep.12240.

57.   Verna, L.; Whysner, J.; Williams, G.M. N-nitrosodiethylamine mechanistic data and risk assessment: bioactivation, DNA-adduct formation, mutagenicity, and tumor initiation. *Pharmacol. Ther.* **1996**, *71*, 57–81, doi:10.1016/0163-7258(96)00062-9.

58.   Li, S.; Ghoshal, S.; Sojoodi, M.; Arora, G.; Masia, R.; Erstad, D.J.; Lanuti, M.; Hoshida, Y.; Baumert, T.F.; Tanabe, K.K.; Fuchs, B.C. Pioglitazone reduces hepatocellular carcinoma development in two rodent models of cirrhosis. *J. Gastrointest. Surg.* **2019**, *23*, 101–111, doi:10.1007/s11605-018-4004-6.

59.   Hayes, J.D.; Dinkova-Kostova, A.T.; Tew, K.D. Oxidative stress in cancer. *Cancer Cell* **2020**, *38*, 167–197, doi:10.1016/j.ccell.2020.06.001.

60. Semenza, G.L. Hypoxia-inducible factor 1: regulator of mitochondrial metabolism and mediator of ischemic preconditioning. *Biochim. Biophys. Acta* **2011**, *1813*, 1263–1268, doi:10.1016/j.bbamcr.2010.08.006.

61. Warburg, O. On the Origin of Cancer Cells. *Science* **1956**, *123*, 309–314, doi:10.1126/science.123.3191.309.

62. Vander Heiden, M.G.; Cantley, L.C.; Thompson, C.B. Understanding the Warburg effect: the metabolic requirements of cell proliferation. *Science* **2009**, *324*, 1029–1033, doi:10.1126/science.1160809.

63. Dong, S.; Liang, S.; Cheng, Z.; Zhang, X.; Luo, L.; Li, L.; Zhang, W.; Li, S.; Xu, Q.; Zhong, M.; et al. ROS/PI3K/Akt and Wnt/β-catenin signalings activate HIF-1α-induced metabolic reprogramming to impart 5-fluorouracil resistance in colorectal cancer. *J. Exp. Clin. Cancer Res.* **2022**, *41*, 15, doi:10.1186/s13046-021-02229-6.

64. Wakiyama, K.; Kitajima, Y.; Tanaka, T.; Kaneki, M.; Yanagihara, K.; Aishima, S.; Nakamura, J.; Noshiro, H. Low-dose YC-1 combined with glucose and insulin selectively induces apoptosis in hypoxic gastric carcinoma cells by inhibiting anaerobic glycolysis. *Sci. Rep.* **2017**, *7*, 12653, doi:10.1038/s41598-017-12929-9.

65. Shi, L.; Zhang, G.; Zheng, Z.; Lu, B.; Ji, L. Andrographolide reduced VEGFA expression in hepatoma cancer cells by inactivating HIF-1α: The involvement of JNK and MTA1/HDCA. *Chem. Biol. Interact.* **2017**, *273*, 228–236, doi:10.1016/j.cbi.2017.06.024.

66. Shirozu, K.; Hirai, S.; Tanaka, T.; Hisaka, S.; Kaneki, M.; Ichinose, F. Farnesyltransferase inhibitor, tipifarnib, prevents galactosamine/lipopolysaccharide-induced acute liver failure. *Shock* **2014**, *42*, 570–577, doi:10.1097/SHK.0000000000000239.

67. Cousin, S.P.; Hügl, S.R.; Wrede, C.E.; Kajio, H.; Myers, M.G.; Rhodes, C.J. Free fatty acid-induced inhibition of glucose and insulin-like growth factor I-induced deoxyribonucleic acid synthesis in the pancreatic beta-cell line INS-1. *Endocrinology* **2001**, *142*, 229–240, doi:10.1210/endo.142.1.7863.

68. Festing, M.F. On determining sample size in experiments involving laboratory animals. *Lab. Anim.* **2018**, *52*, 341–350, doi:10.1177/0023677217738268.